Photoemission from Aqueous Alkali-Metal−Iodide Salt Solutions Using EUV Synchrotron Radiation

R. Weber, B. Winter,* P. M. Schmidt, W. Widdra,† and I. V. Hertel‡

Max-Born-Institut für Nichtlineare Optik und Kurzzeitspektroskopie, Max-Born-Strasse 2A, D-12489 Berlin, Germany

M. Dittmar and M. Faubel

Max-Planck-Institut für Strömungsforschung, Bunsenstrasse 10, D-37073 Göttingen, Germany

Received: June 18, 2003; In Final Form: January 5, 2004

The valence band photoemission of aqueous alkali-metal halide solutions is studied for photon energies from 90 to 110 eV. A 6 μm diameter liquid microjet provides a free vacuum surface, allowing water molecules to evaporate without collisions, and hence enables the direct detection of photoelectrons originating from the liquid. The experiments were performed at the MBI undulator beamline of the synchrotron radiation facility BESSY. Here, we focus on the determination of electron binding energies of solvated anions and cations. The effect of different countercations (Li^+, Na^+, K^+, and Cs^+), and salt concentrations is systematically investigated. Electron binding energies of the solvated ions are found to differ considerably from those in the gas phase; contrary to intuition, the energies do not depend on the salt concentration. Measured binding energies can be surprisingly well explained within a simple dielectric cavity model. For a NaI aqueous solution, negative surface excess is inferred from the evolution of the ion photoemission signal as a function of the salt concentration.

A. Introduction

Water is an excellent solvent due to its polarity, high dielectric constant, and small size, particularly for polar and ionic compounds and salts.[1−4] Water is known to form highly organized intermolecular networks through hydrogen bonding (H bonding) making it sufficiently ionic to separate and insulate some cations from the corresponding anions in a solution. In the case of aqueous solvation the interplay of several processes leads to the formation of solvation shells, implying a considerable reorganization of the water structure.[2−4] Despite their importance, aqueous solutions constitute one of the less understood interactions in chemical physics.[5,6] One reason for this is the difficulty to correctly account for the polarizability of water, and likewise for the polarizability of solvated ions;[7] this property is crucial for treating the respective interaction energies.[6,8,9] A related aspect is ion-pairing in salt solutions, referring to a solvation structure in which a fraction of solvent water molecules is shared by an anion and a cation.[4,7,10] Furthermore, highly polarizable ions have been predicted to have a propensity for the surface which may have consequences for the anion vs cation concentration profile at the very near solution surface and may hence affect the surface (atmospheric) chemistry.[11,12]

Photoelectron spectroscopy is reasonably surface-sensitive, which makes this technique an attractive tool for studying surfaces in detail, including liquid surfaces. In the present work photon energies of 90−110 eV are used, corresponding to an information depth (electron mean free path) of about two to three layers. For a long time photoemission was hardly applicable to *highly volatile* liquids because of the difficulty to transfer photoelectrons from the liquid surface through the vapor phase to an electron detector. This has imposed serious limitations to accessing the electronic structure of liquids. Nevertheless, ionization *threshold* energies were reported some 20 years ago for a number of inorganic cations and anions in aqueous solution.[13−15] Electron spectroscopy for chemical analysis (ESCA) was applied for liquids and solutions having sufficiently low vapor pressures.[16,17] Technical aspects of liquid ESCA were discussed by these authors, and also the concept of interpreting electron binding energies from the liquid phase was presented, which requires a thorough account of liquid electrochemistry and liquid-specific energy shifts.[16,17] For water and *aqueous* ions, the only photoemission data from lower valence levels has been reported for a similar microjet setup as in the present work, using HeI line radiation for excitation.[18] With this laboratory photon source, the outer three valence orbital energies of liquid water, as well as binding energies of some aqueous ions, have been measured for the first time.[19] However, due to a large background of secondary electrons in the spectra, peak positions could not be determined precisely. For the present study the microjet apparatus has been modified for the use at a synchrotron radiation source. When compared to the HeI low-energy photons, tunable undulator radiation is beneficial for several reasons: the range of binding energies which can be studied is dramatically increased with energies well below the valence levels now being accessible, and the information depth may be changed by variation of the photon energy. Also, as we have demonstrated recently for pure liquid water,[20] the use of polarized photons of tunable energy is very

* Corresponding author. E-mail: bwinter@mbi-berlin.de.
† Present address: Martin-Luther-Universität Halle-Wittenberg, Halle, Germany.
‡ Also at Freie Universität Berlin, Berlin, Germany.

10.1021/jp030776x CCC: $27.50
Published on Web 03/18/2004

valuable for the interpretation of photoionization cross sections and molecular orbital structural changes related to it. Recently, the liquid microjet technology has also been applied to study the water/vapor[21] and the methanol/vapor interfaces[22] under high vacuum conditions by near-edge X-ray absorption fine structure (NEXAFS) and extended X-ray absorption fine structure (EXAFS) spectroscopy.

In the present experiment we report photoemission spectra from aqueous alkali-metal iodide solutions obtained for photon energies between 90 and 110 eV, taking advantage of the I^-(4d) shape resonance near 100 eV photon energy[23] which considerably increases the iodide detection sensitivity. The experiments aim at a better understanding of the structure of hydrated anions and cations. In particular, experimental electron binding energies of solvated ions may be related to structural details of hydration shells. The photon energies available enable the determination of electron binding energies well above threshold, which have not been accessed previously. Note that many aqueous cations of interest, for instance solvated alkali-metal cations with their closed-shell configuration, possess electron binding energies larger than 20 eV. The effect of a counterion (Li^+, Na^+, K^+, and Cs^+) on the electron binding energy of iodide in the respective metal-halide solution will be evaluated. The concentration dependence of the photoemission spectra from NaI aqueous solutions, reported here, explores if there are different ion densities for anions vs cations in the interface (anion surface excess)[7] and if overall ion concentrations in the subsurface region are lower than in the bulk solution.[11,12]

B. Experimental Section

A liquid micrometer-sized water jet, 6 μm in diameter, was generated in a high-vacuum environment in order to make photoelectron spectroscopy applicable to a highly volatile liquid. This small beam size results in nearly collisionless evaporation.[24] A detailed description of the setup has been given elsewhere.[20] In short, the jet, having a temperature of 4 °C, is formed by injecting the liquid at 80 bar He pressure through a 10 μm diameter orifice.[25] At the exit of the nozzle the beam contracts to 6 μm[18,19,25] and acquires a final velocity of about 125 ms^{-1}. For 3−5 mm downstream from the nozzle, the beam is laminar having a smooth surface. The working pressure in the main chamber containing the jet is 10^{-5} mbar. Photoelectrons pass through a 100 μm orifice, which separates the main chamber from the electron detection chamber. The latter is equipped with a hemispherical electron energy analyzer (Specs/Leybold EA 10/100) and a single electron multiplier detector for electron counting. Highly demineralized water was used in the experiments, and salts were of highest quality commercially available.

The photoemission measurements were performed at the MBI−BESSY undulator beamline (U125), providing photon energies up to about 180 eV at an energy resolution better than 6000. For the present experiments, the resolution was reduced in favor of the photoemission signal to about 100 meV, which is more than sufficient for the observed structures considering their intrinsic width of typically >0.5 eV. At a photon flux of about 4×10^{12}/s per 0.1 A ring current, count rates on the order of 10−100 counts per second at peak maximum were obtained. The synchrotron light intersects the laminar liquid at normal incidence. Then, electron detection is normal to both the jet direction and the light polarization vector.

C. Results and Discussion

Solvent and Solute Features. Photoelectron spectra of pure liquid water and of 1 *m* aqueous NaI solution, obtained for 100 eV excitation photon energy, are displayed as the bottom and top traces in Figure 1, respectively. Typical acquisition time per spectrum is about 30 min. For clarity the spectra are vertically displaced relative to each other, with the intensities normalized to the H_2O $1b_1$ emission signal from liquid water (see below). The abscissa in the figure is the electron binding energy relative to vacuum. In our recent work on liquid water, the binding energy of the $1b_1$ water orbital was shown to be 11.16 eV.[20]

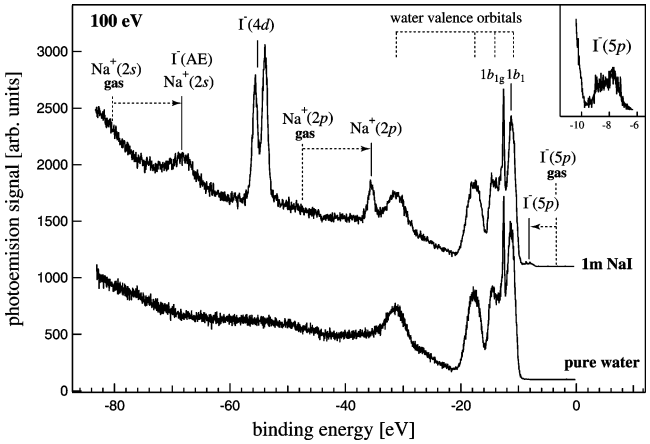

Figure 1. Photoemission spectra of liquid water (bottom) and of 1 *m* NaI aqueous solution (top), obtained for 100 eV photon energy. Energies are given with respect to the vacuum level. The vertical dashed lines indicate the binding energy of the respective gas-phase ion, and the arrows indicate the direction of the gas−liquid shift. The emission from the aqueous ions is labeled. The inset shows an enlargement of the emission onset (threshold).

Comparing the photoemission spectra obtained for 1 *m* salt solution with the one for pure water, one can recognize the underlying water features along with the peaks arising from the alkali-metal and iodide ions. The energetic positions of the characteristic water valence orbitals are marked at the top of the figure. From left to right, these correspond to the emission from liquid water's $2a_1$, $1b_2$, $3a_1$, and $1b_1$ molecular orbitals, respectively.[20] Gas-phase emission contributions in our spectra, particularly noticeable at the position labeled $1b_{1g}$, result from the continuous evaporation of the liquid surface. The broad background largely arises from secondary electrons; additional distinct features, e.g., near 50 eV binding energy, can be assigned to specific electron energy losses.[20] Iodide photoemission gives rise to the weak low-energy doublet feature at 7.7/8.8 eV (see inset in the top right corner of Figure 1), the strong doublet at 53.8/55.5 eV, and in part, to the broad feature near 68 eV. These peaks can be assigned to I^-(5p), $I^-(4d_{5/2,3/2})$ direct emission, and Auger electrons, respectively. The large I^-(4d) photoemission signal is due to a shape resonance peaking near 100 eV photon energy. A discussion of this resonance for *solvated* iodide, in comparison with gas-phase data,[23] can be found elsewhere.[26]

Indicated by dashed vertical lines are the corresponding gas-phase binding energies of the ions as found in the literature.[23,27,28] Notice that electron binding energy shifts, with respect to the gas-phase ion, are considerably different for solvated cations and anions. For instance, the aqueous sodium ion exhibits a solvation energy shift of about 12 eV toward lower binding energies, from 47.3 to 35.4 eV for Na^+(2p), while the iodide energy shift, from 3.1 to 7.7 eV for I^-(5p), is smaller and in the opposite direction. The reason for these differences, and also the origin of peak broadening, will be discussed below.

Effect of Counteranion. Photoemission spectra from aqueous solutions of 3 *m* LiI, 3 *m* NaI, 3 *m* KI, and 2 *m* CsI, respectively,

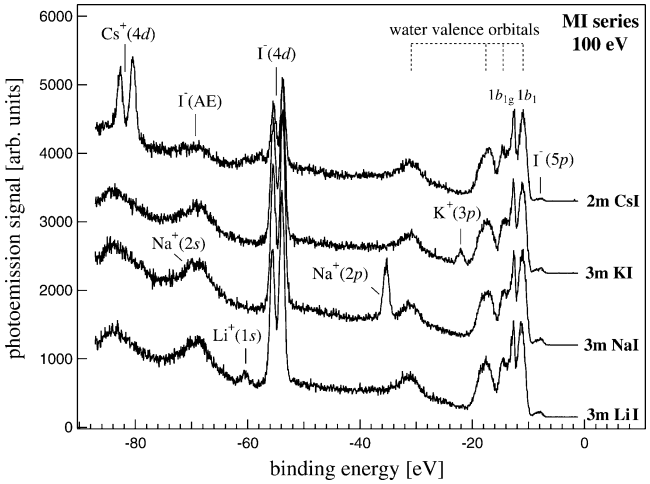

Figure 2. Photoemission spectra of aqueous alkali-iodide solutions (LiI, NaI, KI, CsI) obtained for 100 eV photon energy. The (molal) concentrations of the solutions are indicated.

TABLE 1: Measured Electron Binding Energies (E_{aq}^{PES}) of Aqueous Alkali-Metal Ions and Peak Widths ($fwhm_{aq}$) of the Corresponding Photoemission Features[a]

atom M		$E_g(M^\circ)$ (eV)	$E_g(M^+)$ (eV)	$fwhm_{aq}$ (eV)	$E_{aq}^{PES}(M^+)$ (eV)	$E_{aq}(M^+)$ (eV)
Li	2s	5.39				
	1s[b]	64.42	75.64[f]	1.4 ± 0.20	60.4 ± 0.07	59.44
		66.31				
Na	3s	5.14				
	2p[c]	37.98	47.28[f]	1.1 ± 0.03	35.4 ± 0.04	34.65
		38.07	47.45[f]			
		38.14				
		38.45				
	2s	71.03	80.07[f]	3.1 ± 0.50	68.0 ± 0.15	67.44
K	4s	4.34				
	3p[c]	24.48				
		24.57	31.62[f]	1.4 ± 0.20	22.2 ± 0.06	21.60
		24.81	31.89[f]			
	3s[d]	24.97				
		41.00	47.81[f]			
Cs[e]	6s	3.89				
	5p	17.23	23.14[g]			14.53
		17.64				
		19.06				
		19.12				
	5s	30.65				
	$4d_{5/2}$	82.74	88.55[g]	1.1 ± 0.05	80.6 ± 0.03	79.94
	$4d_{3/2}$	85.01		1.3 ± 0.06	82.9 ± 0.04	

[a] Also shown are the calculated electron binding energies (E_{aq}) of aqueous alkali metal ions as well as gas-phase energies (E_g) of both neutrals and ions. [b] Reference 29. [c] Reference 30. [d] Reference 31. [e] Reference 32. [f] Reference 27. [g] Reference 33.

obtained for 100 eV photons, are displayed in Figure 2. The lower concentration used for the latter solution is due to the low solubility of CsI in water. Again, spectra are vertically displaced relative to each other, intensities are normalized to the H_2O $1b_1$ peak height (liquid), and electron binding energies are relative to vacuum. As shown above iodide photoemission gives rise to the weak doublet and the strong doublet features at 7.7/8.8 and 53.8/55.5 eV, respectively. This energy is found to be independent of the countercation. Notice that intensities of solute features in Figure 2 correlate with the respective salt concentrations.

The new features in the spectra originate from alkali ion emission and can be assigned as follows (see Table 1). $Li^+(1s)$ emission results in a peak at 60.4 eV binding energy, and the two features corresponding to $Na^+(2p)$, $Na^+(2s)$ appear at 35.4

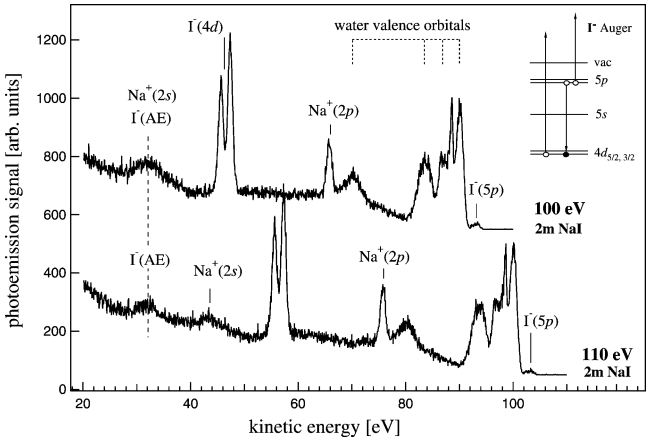

Figure 3. Photoemission spectra of aqueous NaI solutions (concentrations as shown) for 100 (top) and 110 eV (bottom) photon energy. Electron energies are displayed on the kinetic energy scale. Iodide 4d−5p5p Auger features (AE), at constant kinetic energy (near 32 eV), are marked by the dashed vertical line. The inset is a schematic of the transitions involved in the Auger process.

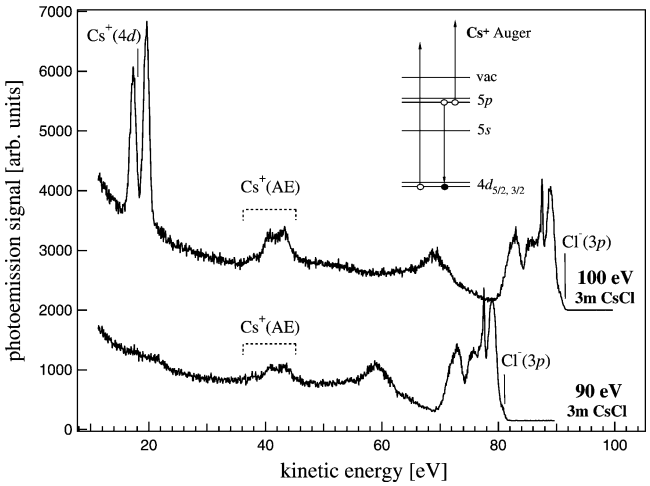

Figure 4. Photoemission spectra of aqueous CsCl solutions for 90 and 100 eV photon energy, as labeled. Electron energies are displayed on the kinetic energy scale. Cesium 4d−5p5p Auger features appear near 40 eV. The inset is a schematic of the transitions involved in the Auger process.

and 68.0 eV, respectively. For the KI solution, the new peak at 22.2 eV arises from $K^+(3p)$, and the intense doublet at 80.6/82.9 eV for the CsI solution is due to $Cs^+(4d)$ emission.

Figure 3 shows the partial Auger character of the feature at 68 eV (compare Figure 2) for a 2 *m* NaI solution in water. Notice that independent of the excitation energy (100 vs 110 eV) some emission, though reduced, still contributes at the position corresponding to 68 eV binding energy, while the directly ionized electrons change their kinetic energy with photon energy. The Auger process is assigned to filling the $I^-(4d)$ hole by a $I^-(5p)$ electron, and simultaneous emission of a 5p electron leading to a two-hole final state (4d−5p5p; see inset in Figure 3). The other contribution to the 68 eV feature is attributed to $Na^+(2s)$ emission. Also the weak feature near 58 eV binding energy in the CsI spectrum (Figure 2) is attributed to an Auger transition, originating from the Cs 4d−5p5p emission process. Similar to the iodide case, the Cs^+ Auger line has also been identified by variation of the photon energy. This is shown in Figure 4, comparing the photoemission spectra (on a kinetic energy scale) of a 3 *m* CsCl aqueous solution obtained for 90 and 100 eV, respectively. To better discern the Cs^+ Auger

TABLE 2: Electron Binding Energies of Iodide, in Aqueous Solution (E_{aq}) and in the Gas Phase (E_g)[a]

iodine		E_g(I°) (eV)	E_g(I⁻) (eV)	fwhm$_{aq}$ (eV)	E_{aq}^{PES}(I⁻) (eV)	E_{aq}(I⁻) (eV)
I	5p[b]	10.50	3.06[d]	0.8 ± 0.30	7.7 ± 0.20	6.24
		11.31		1.1 ± 0.30	8.8 ± 0.20	
		12.17				
		14.11				
	5s[b]	20.80				18.28
		21.30	15.10*[e]			
	$4d_{5/2}$[c]	57.83		1.0 ± 0.02	53.8 ± 0.03	61.39
	$4d_{3/2}$	59.73	57.41*[e]	1.0 ± 0.02	55.5 ± 0.03	

[a] Identical E_{aq}(I⁻) values were obtained for 2 *m* aqueous alkali-metal−iodide solutions MI (M = Li, Na, K, Cs) as well as for a 2 *m* aqueous CaI_2 solution. The asterisk in the third row indicates theoretical energies, since experimental values are not available. [b] Reference 34. [c] Reference 35. [d] Reference 28. [e] Reference 23. Binding energies E_{aq} are determined from eqs 3 and 3′.

contribution, the anion has been varied in Figure 4 since the Cs^+ Auger line and the I^-(4d) lines strongly overlap at these photon energies. The only chloride contribution observed in our spectra, attributed to Cl^-(3p) emission, gives rise to a weak signal at 9.6 eV electron binding energy. The origin of the very weak feature at 20 eV in the bottom spectrum of Figure 4 is unclear.

In conclusion, the constant electron binding energy of aqueous iodide in different alkali-metal−iodide solutions is consistent with negligible anionic solvation structural changes. This result was observed as well in the case of divalent cations, for example in CaI_2 solutions, not shown here explicitly because the photoemission signal from Ca^{2+} is strongly masked by the water emission signal. The observed absence of any change in electron binding as a function of the salt concentration and for different cation−anion combinations indicates that the solvating water molecules efficiently shield ion−ion interactions. Apparently, for the solutions considered here, individual ions can be assumed to be completely solvated. Similar results were inferred by very different classical experimental methods as discussed in ref 2. Constant electron binding energies are also found for the water orbitals in our studies, irrespective of the solute. Hence, within the limits of the present experiment (30 meV), the electronic structure is indistinguishable between solvate water (both anion and cation solvation) and bulk water; energy shifts would be at most on the order of the peak broadening. Then, the peak widths observed here, typically >1 eV, may be interpreted to reflect a distribution of energies which is associated with different, heterogeneous solvation situations. We would like to remark that in an analogous argument, also for pure liquid water, the peak broadening has been attributed to the existence of different H bonding environments.[20] With that in mind, it may also be worthwhile to mention that the photoelectron spectra of H_2O and D_2O are indistinguishable from each other.[20] This further suggests that the photoelectron peak broadening is due to heterogeneous H and D atom environments rather than arising from lifetime effects associated with the making and breaking of H bonds during the photoemission process.

Discussion of Electron Binding Energies for Aqueous Iodide and Alkali-Metal Cations. Tables 1 and 2 summarize the measured electron binding energies (E_{aq}^{PES}) and peak widths (fwhm$_{aq}$) for alkali-metal cations and the iodide anion obtained here by photoemission. For comparison we also show the relevant gas-phase energies (electron binding energies of both neutrals and the respective ions, E_g) as reported in the literature.[23,27−35] Literature data include the first ($M^\circ + h\nu \rightarrow M^+ + e^-$) and the second ($M^+ + h\nu \rightarrow M^{2+} + e^-$) ionization

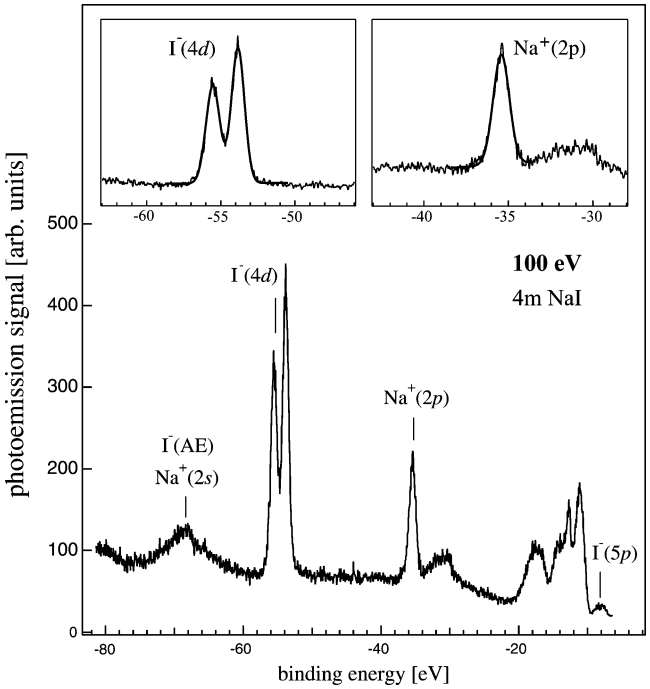

Figure 5. Gaussian fits to the I^-(4d) and Na^+(2p) emission features for a 4 *m* NaI aqueous solution.

potential (IP) of the corresponding gas-phase alkali atom M°. The relevant quantity for the iodide halide would be the first IP of the respective negative atom, IP(I⁻). Finally, the energy required to remove a deeper electron from the respective singly charged atom, i.e., from M^+ and I^-, has also been included when available. The experimental binding energies of aqueous ions, E_{aq}^{PES}, and the corresponding fwhms of the photoemission peaks, reported in Tables 1 and 2 result from individual peak fitting averaged over a number of spectra. A typical fit, exemplified for Na^+ and I^- features in 4 *m* NaI solution, is presented in Figure 5. Binding energy errors given in the tables are statistical errors. These numbers are significantly smaller than the observed peak widths found in the present experiment. As mentioned above, the experimental iodide binding energy, E_{aq}^{PES}(I⁻), reported here is independent of the countercation.

Observed peak widths are significantly broadened as compared to the gas phase. Typical values for fwhm$_{aq}$ are 1.1−1.4 eV, which is very similar to the value for the $1b_1$ orbital of liquid water, 1.4 eV.[20] The peak broadening of this orbital in the liquid phase has been assigned to the existence of different local environments of the H_2O molecule, which correlates to a distribution of binding energies. The exceptional large peak width for Na^+(2s), 3.1 eV, reflects the existence of several close lying photolines, as known from gas-phase measurements.[36]

Electron binding energy shifts, $E_{aq}^{PES} - E_g$, between liquid and gas-phase water correlate with the free energy penalty for disrupting the local solvent structure, known as the solvent reorganization energy.[2,4,9] Additional effects, such as electronic polarization screening, are smaller but not necessarily negligible.[20] *Solvation* contributions can be compared to the experimental Gibbs free energy of solvation, ΔG°. The observed electron binding energies may be theoretically interpreted within a dielectric continuum cavity model originally introduced by Born:[2,17,37]

$$\Delta G^{cav} = -(z^2e^2/8\pi\epsilon_o R)(1 - 1/\epsilon_{st}) \qquad (1)$$

Equation 1 is known as Born's equation[2,17] for the "Lösung-

swärme".[37] Here ΔG^{cav} is the electrostatic free energy, assuming electronic polarization of a continuum solvent about a charge *ze* in a spherical cavity (cav) of radius *R*, with ϵ_o and ϵ_{st} being the static permittivity of vacuum and of the dielectric medium, respectively. The limits of eq 1, along with various modifications, were discussed in detail elsewhere.[2,38] We would like to emphasize that for the present purpose eq 1 will be used to link measured vertical ionization energies and thermodynamic quantities in a simple and convenient manner in order to allow for a rough comparison with our experimental data. Clearly, this simple approach entirely neglects any concentration dependence on the solvation details. For the present discussion, the numerical choice of *R* is not as relevant since we will relate electron binding energies, measured by photoemission, to *experimental* (thermochemical) values of the solvation free energy; this will be discussed below. However just to briefly mention it, approximating *R* by an effective radius $R_{eff} = (R_{ion}^{crystal} + r_{gmax})/2$, for instance, turned out to fit the experimental data reasonably well.[39] Here R_{ion} is the crystal ionic radius, and r_{gmax} is the shortest interatomic distance between an ion and a water molecule (see, e.g., ref 2). The latter is derived from the first minimum of the pair-correlation function $g_{ij}(r)$.[2]

To properly apply eq 1 to the present experiment the relevant photoionization processes need to be considered in detail:

$$M^+_{aq} + h\nu \rightarrow M^{2+}_{aq} + e^-_{vac} \quad (2)$$

$$I^-_{aq} + h\nu \rightarrow I^\circ_{aq} + e^-_{vac} \quad (2')$$

The energies required for the processes involved in eqs 2 and 2′ are the vertical ionization energies, which are measured here. Since the photoemission process is much faster than the time scale required to reorganize the initial solvation shell, the photoelectron carries only the information on the original solvation configuration; it does not sense reorientational changes of the solvent molecules. Consequently, the static permittivity may be used in eq 1.

The experimental value for the electron binding energy of a given ion in solution, E_{aq}^{PES} (see Tables 1,2), may be approximated by E_{aq}^* given by $E_{aq}^* - E_g = \Delta G^*$, where the asterisk indicates that this value is based on eq 1. Notice that the expression for E_{aq}^* contains electron binding energies as well as free energies. This is justified since entropy changes may be neglected on the time scale of photoionization, as was mentioned above. According to eqs 2 and 2′, one needs to account for the solvation energies of both the respective initial and final states of a given anion or cation in solution, ΔG_i^{cav} and ΔG_f^{cav}, yielding $\Delta G^* = \Delta G_f^{cav} - \Delta G_i^{cav}$. Hence, with eqs 2 and 2′, one derives expressions for ΔG^* for both anions and cations:

$$\Delta G^*(\text{anion}) = (-e^2 0^2 - (e^2(-1)^2)\{(1/8)\pi\epsilon_o R)(1 - 1/\epsilon_{st})\} = (e^2/8\pi\epsilon_o R)(1 - 1/\epsilon_{st}) = \Delta G^{cav} \quad (3)$$

$$\Delta G^*(\text{cation}) = (-e^2 2^2 - (-e^2 1^2)\{(1/8)\pi\epsilon_o R)(1 - 1/\epsilon_{st})\} = -3(e^2/8\pi\epsilon_o R)(1 - 1/\epsilon_{st}) = -3\Delta G^{cav} \quad (3')$$

As a result of the photoemission process, *z* changes from −1 to 0 for anionic solvation and from +1 to +2 for cationic solvation which, according to (3,3′), leads to different energy shifts (with respect to both direction and magnitude). Electron binding energies E_{aq}^* ($=\Delta G^* + E_g$) thus increase for anions but decrease for cations with respect to the corresponding gas-phase value. This situation, depicting the energies of the respective species involved, is illustrated in Figure 6. To evaluate (3,3′) quantitatively, experimental values of the solvation free energies,[40] ΔG° (rather than ΔG^{cav}, which would require a value for *R*), have been used: −521, −406, −322, −277, and −307 kJ/mol for Li^+, Na^+, K^+, Cs^+, and I^-, respectively. Energies, E_{aq}, determined this way, are given in Tables 1 and 2. For cations, the energies E_{aq}^{PES} and E_{aq} typically agree to within less than 1 eV, rather surprisingly for such a simple model. The agreement for the iodide anion is less satisfactory. E_{aq}^{PES} and E_{aq} for I^-(5p) differ by ca. 1.5 eV (7.7 vs 6.2 eV), and for I^-(4d), E_{aq}^{PES} is even *smaller* than E_{aq}, by >6 eV.

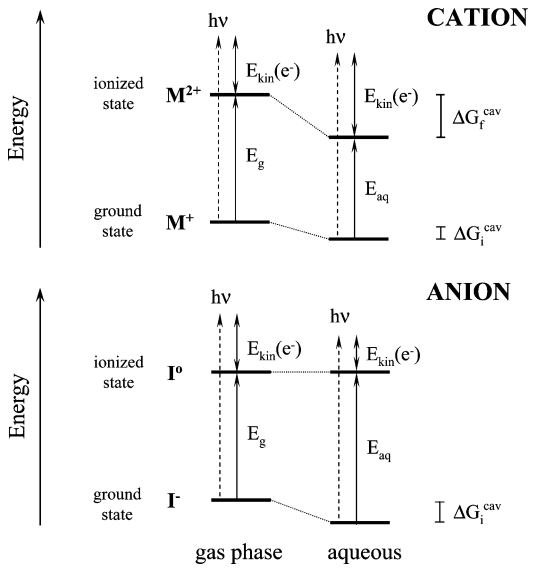

Figure 6. Schematic energy level diagrams illustrating the liquid-phase binding energy shifts in terms of the solvation free energy, $\Delta G_{i,f}$ (for initial and final state), relative to the respective gaseous ion. E_g and E_{aq} are the electron binding energies of the gas-phase species and the hydrated species, respectively. The different direction of the gas−liquid shifts for solvated cations (top) vs anions (bottom) can be directly inferred from the lengths of the arrows (labeled E_{aq} and E_g). Also shown is the measured kinetic energy of the electrons, E_{kin}, for a given photon energy.

Also for chloride, not shown in the table, energies differ by ca. 2 eV: $E_{aq}^{PES}(Cl^-(3p)) = 9.6$ eV and $E_{aq}(Cl^-(3p)) = 7.59$ eV; we have used −384 kJ/mol[40] for the solvation energy of Cl^-. The better agreement for cation solvation is likely to reflect the fact that orientation changes of the solvation shell are only small for ionization of a cation; in this case both the initial and final state corresponds to cationic solvation. In the other case, the disturber changes from anion to neutral.[13,14] Notice, however, that the large discrepancy, observed for the gas−liquid shift of the prominent 4d energy level for iodide, may be well attributed to the fact that the corresponding gas-phase value is not yet precisely known. The value assumed in Table 2 is a theoretical one.[23] There may well also be other effects that should be taken into account, such as ion polarizability, which is not explicitly included in the simple cavity model. The effect would be smallest for the alkali-metal cations with no valence electrons, while the halide anion is significantly stronger polarizable.[41]

In any case, the continuum model used here does not assume any microscopic details of the solvation shell structure, and strictly speaking, the cavity (Born) model is applicable only for distances considerably larger than the ion radius. A microscopic description has to account for the specific interactions of a water molecule with the two types of ions; obviously there are differences as to the role of H bonding for the two cases. For cationic solvation, the O−H groups point away from

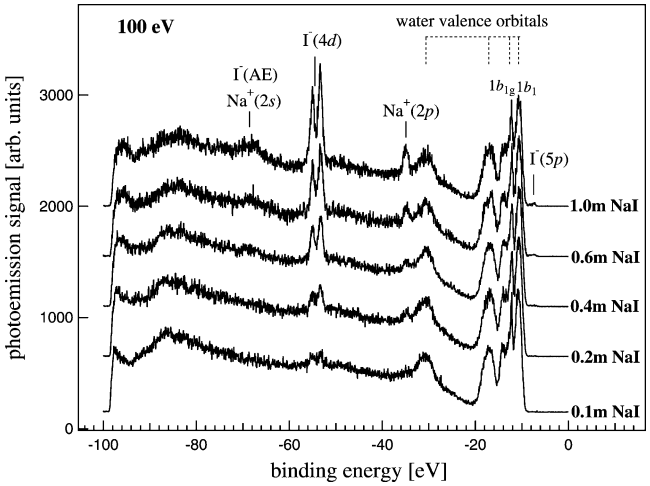

Figure 7. Photoemission spectra of NaI aqueous solution obtained for different salt concentrations, from 0.1 to 1.0 *m*, as labeled. Intensities have been normalized to the synchrotron photon flux. The photon energy was 100 eV.

the ion (then the oxygen atom points to the ion) in order to form O−H···H hydrogen bonds with bulk water molecules at the solvation shell boundary. For anions, the water molecules are bound by directional O−H···Y− hydrogen bonds; water−halide H bonds are stronger than water−water H bonds.[11] This may well alter the effective dipole moment associated with stabilizing the solvation shell. We are currently studying the electron binding energies of gas-phase alkali halides, $Cs^{\delta+}Y^{\delta-}$ and $M^{\delta+}I^{\delta-}$, as these systems may be useful to better understand the electronic interactions in ion solvation by water. At this point it is interesting to note that, for example, the Cs^+(4d) binding energy for the aqueous ion and the gas-phase molecules agree on average to within 1.5 eV. This is similarly true for the I^-(4d) binding energy; however, as mentioned above, no experimental value exists for the gas-phase iodide.

High vs Low Concentration: Aqueous NaI Solution. At 100 eV photon energy, corresponding to the maximum of the shape resonance in the I^-(4d) photoionization cross section of aqueous iodide,[26] the iodide signal may be detected in the present experiment for a concentration as low as 0.1 *m* (e.g., in aqueous NaI and much lower for surface-active iodine containing salts). Hence, the evolution of the photoemission spectra can be followed over a large range of concentrations, up to saturation, which is about 13 *m* for aqueous NaI solutions. In principle, the study of electron binding energies and intensities of emitted electrons, as a function of the concentration, should provide details of the solution surface. Specifically, one might expect binding energy changes for varying (solvation) coordination numbers, which could be different for bulk vs surface ions (partial solvation). We would like to point out, though, that the present experiment requires rather high concentrations, for which ions are no longer perfectly separated by the polar solvent molecules (Debye−Hückel model for electrolytes[42]). Instead, some type of solvent-shared solvation structure[4,6,7,10] must exist, having consequences for the relative distribution of anions vs cations near the surface, even for concentration changes in the regime >0.1 *m*.[11]

Figures 7 and 8 display photoemission spectra of aqueous NaI solutions for the low (0.1−1.0 *m*) and high (0.5−12 *m*) salt concentration range, respectively. The spectra are vertically displaced with respect to each other and are normalized relative to the synchrotron ring current; i.e., to the photon flux. Great care has been taken to maintain constant experimental conditions for obtaining all spectra in each figure as this allows the accurate

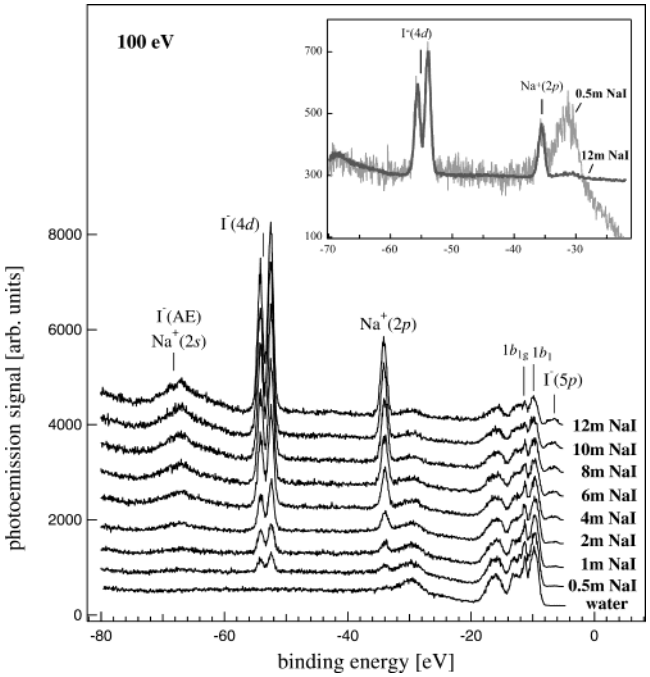

Figure 8. Photoemission spectra of NaI aqueous solution obtained for different salt concentrations, 0.5−12 *m*. The excitation photon energy was 100 eV. Intensities have been normalized to the synchrotron photon flux. The inset displays the spectra of lowest and highest salt concentration, on top of each other, scaled for identical intensities. From this comparison constant electron binding energies of both I^-(4d) and Na^+(2p) as a function of the salt concentration are inferred.

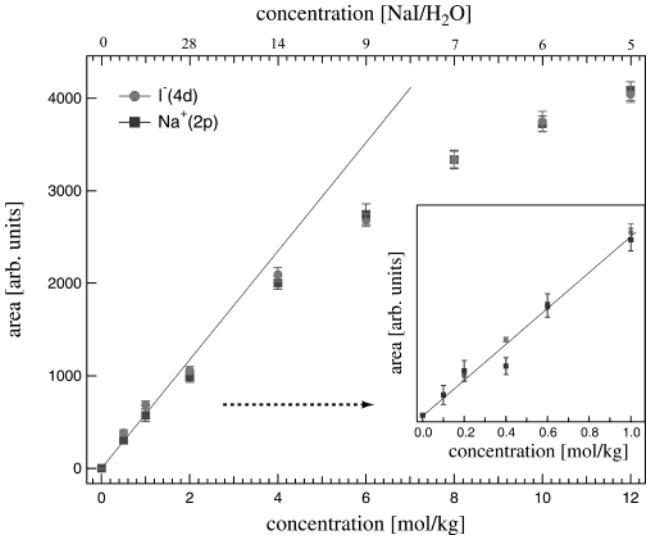

Figure 9. Increase of the I^-(4d) and Na^+(2p) photoemission signal as a function of the NaI concentration (based on peak fitting and integration of spectra in Figures 7,8). The inset presents data for low concentrations, up to 1.0 *m*. The sublinear increase for concentrations larger than 2 *m* is attributed to a slower increase of ions near the surface as compared to the bulk solution.

assignment of the ring current to the intensity of a given photoemission spectrum. This is crucial for accessing *absolute* signal attenuation/increase for varying salt concentration. To infer the emission intensities of both ions as a function of the concentration, the corresponding peak integrals (based on Gaussian peak fitting) of the I^-(4d) and the Na^+(2p) features have been evaluated. The result is presented in Figure 9. The main figure shows the photoemission intensities for both anions and cations over the full range of concentrations, whereas the inset displays data for the lower concentrations only. Our data

indicate no differential behavior of the ion intensities since the anion to cation signal ratio remains constant. Hence the present result will not necessarily support any surface excess of anions as theoretically predicted for aqueous NaI (and other sodium halides) at the air/solution interface.[11,41] Yet, such an enhancement of the anion concentration at the interface cannot be ruled out because the surface sensitivity of the present experiment, a few layers, would still be insufficient to resolve density profile changes within a region being small compared to the electron information depth. Indeed, molecular dynamics (MD) simulations predict that at the interface of a NaI aqueous solution highest anion and cation densities are separated by a distance which is smaller than the diameter of one water molecule.[11]

The observed saturation behavior of the ion signal for concentrations above 2 *m* NaI concentration, see Figure 9, is indicative of ion surface "depletion" (i.e., bulk ion concentration increases faster than the ion concentration near the surface). Lower ion density at the surface suggests that for near-saturation a larger number of ions can be stabilized by solvation shells in the bulk, as compared to the surface. High concentrations of ions may only exist in the bulk as dipole interactions between neighboring solvated ions are fully averaged out. At the surface, the effect is reduced because of unbalanced interactions. This result would be consistent with a depletion of ions in the subsurface region, in qualitative agreement with the aforementioned MD simulations.[11] The effect is related to solute-induced surface tension changes, which can be described by the Gibbs adsorption equation.[43] Then, the increase of surface tension of "hard" water corresponds to negative adsorption of the ions, which in turn correlates with lower ion concentrations near the interface than in the bulk solution.[12,43] This thermodynamic description (Gibbs equation) cannot be used, however, to infer the molecular structure of the interface. The depletion region may possess a characteristic ion density profile. As mentioned, I^- is likely to be enriched right at the interface (iodide surfactant activity), as compared to cations.[11,44] Yet, the overall ion concentration would still be lower in the subsurface region than in the bulk, but for neutrality equal amounts of anions and cations must exist. This can be seen qualitatively in ref 11, even though the interaction potentials used need to be improved in order to reach full convergence of the simulation. As mentioned, these microscopic structural details (negative surface excess) cannot be discerned in the present experiment.

The peak positions of both Na^+ and I^- features are found to be strictly constant to within ±30 meV for all concentrations studied in an extended range over more than 2 orders of magnitude. This is concluded from thorough peak fitting of the individual spectra as exemplified in Figure 5. The striking experimental evidence for constant cation and anion peak positions is further illustrated by the inset in Figure 8, where zero peak shift for low vs high concentration can be directly inferred by comparison of the photoemission spectra of 0.5 and 12 *m* NaI aqueous solutions. The spectra are plotted with normalized amplitude as a light gray and as a heavy line, respectively. We note at this point that 12 *m* concentration corresponds to a ratio of water-to-salt molecules of about 5:1, which only allows for shared solvation shells; the situation is certainly well beyond the Debye−Hückel description. This brings up the question why do not we observe a peak shift; is it possibly masked? Intuitively, electron binding energies might be expected to correlate with the change of solvation shell coordination. However, recent extended molecular simulations of solvated iodide [44] show that the electron binding energy of iodide at the interface is only slightly greater, by about 0.06 eV, than for iodide burried in the interior (7.176 vs 7.050 eV which is about 0.6 eV smaller than $E_{aq}^{PES}(I^-)$). This has been attributed to the balance of reduced binding of surface solvated iodide, to one or two water molecules in the first solvation shell, and the gain in polarizability of asymmetrically solvated surface iodide.[44] Therefore, the detachment energy is *not* sensitive to the position.

We note here in passing a possibly related observation. Ionization potentials of $Na^+(H_2O)_n$ clusters are known to be independent of the cluster size for $n \geq 4$,[45] which was attributed to a fortuitious compensation of several contribution to the solvation energy.[46] The same holds for other alkali-metal−water clusters.[47] On the other hand is the observation of constant binding energy consistent with the existence of a surface repulsion layer in which full-shell solvation is maintained by keeping ions away from the liquid/vacuum boundary. It is noteworthy, however, that surface solvation has been suggested to occur in clusters, e.g., $I^-(H_2O)_n$.[48]

We conclude by noticing that the increase of the ion concentration also correlates with the attenuation of the water signal, by about 40% for the high-concentration solutions with respect to pure water (Figure 8). Since the electron mean escape depth,[20] using 100 eV photons, is on the order of the dimension of the subsurface region, this decrease of the water signal can be attributed to the replacement of water molecules by salt within the near-surface region.

Conclusion and Summary

Electron binding energies were determined for aqueous iodide and alkali ions in the range 7−82 eV. Solvated alkali ions exhibit solvation shifts up to 16 eV toward lower binding energies, while considerably smaller shifts, in the opposite direction, are observed for aqueous iodide. Absolute electron binding energies can be reasonably well reproduced using a simple continuum model. Within the limits of the present photoemission experiment the iodide binding energies were identical for the solutions studied, i.e., no countercation effect was observed. Likewise, electronic structural differences for solvation-shell water for both solvate anions and cations vs bulk water are indistinguishable within present experimental accuracy. The spectra obtained for NaI aqueous solutions, over a wide range of concentrations, suggest that for sufficiently high concentrations the near-surface ion density is smaller than that in the bulk. Enrichment of anions over cations at the surface could not be explicitly identified, and furthermore, constant electron binding energies were measured for anions and cations over an extended range of salt concentrations.

Acknowledgment. We would like to acknowledge the continuing friendly support of the BESSY staff, particularly by R. Follath, G. Reichardt, and W. Braun. We also thank P. Jungwirth for stimulating discussions.

References and Notes

(1) Platzmann, R.; Franck, J. *Z. Phys.* **1954**, *138*, 411.
(2) Marcus, Y. *Chem. Rev.* **1988**, *88*, 1475.
(3) Ohtaki, H.; Radnai, T. *Chem. Rev.* **1993**, *93*, 1157.
(4) Barthel, J. M. G.; Krienke, H.; Kunz, W. *Physical Chemistry of Electrolyte Solutions*; Steinkopff Verlag GmbH & Co., KG: Darmstadt, Germany, 1998.
(5) Kropman, M. F.; Bakker, H. J. *J. Chem. Phys.* **2001**, *115*, 8942.
(6) Carignano, M. A.; Karlström, G.; Linse, P. *J. Phys. Chem.* **1997**, *101*, 1142.
(7) Jungwirth, P.; Tobias, D. J. *J. Phys. Chem. B* **2000**, *104*, 7702.
(8) Silvestrelli, P.; Parrinello, M. *Phys. Rev. Lett.* **1999**, *82*, 3308.
(9) Levine, I. N. *Quantum Chemistry*; Challice, J. Ed.; Prentice Hall: Upper Saddle River, NJ, 2000.

(10) Degreve, L.; da Silva, F. L. *J. Chem. Phys.* **1999**, *110*, 3070.
(11) Jungwirth, P.; Tobias, D. J. *J. Chem. Phys. B* **2001**, *105*, 10468.
(12) Jungwirth, P.; Tobias, D. J. *J. Phys. Chem. B* **2002**, *106*, 6361.
(13) Watanabe, I.; Flanagen, J. B.; Delahay, P. *J. Chem. Phys.* **1980**, *73*, 2057.
(14) von Burg, K.; Delahay, P. *Chem. Phys. Lett.* **1981**, *78*, 287.
(15) Delahay, P.; von Burg, K.; Dziedzic, A. *Chem. Phys. Lett.* **1981**, *79*, 157.
(16) Siegbahn, H. *J. Phys. Chem.* **1985**, *89*, 897.
(17) Lundholm, M.; Siegbahn, H.; Holmberg, S.; Arbman, M. *J. Electron Spectrosc. Relat. Phenom.* **1986**, *40*, 163.
(18) Faubel, M.; Steiner, B.; Toennies, J. P. *J. Chem. Phys.* **1997**, *106*, 9013.
(19) Faubel, M. *Photoionization and Photodetachment, Part I*; Ng, C. Y., Ed.; World Scientific: Singapore, 2000.
(20) Winter, B.; Weber, R.; Widdra, W.; Dittmar, M.; Faubel, M.; Hertel, I. V. *J. Phys. Chem.* , in press.
(21) Wilson, K. R.; Rude, B. S.; Catalano, T.; Schaller, R. D.; Tobin, J. G.; Co, D. T.; Saykally, R. J. *J. Phys. Chem. B* **2001**, *105*, 3346−3349.
(22) Wilson, K. R.; Schaller, R. D.; Co, D. T.; Saykally, R. J.; Rude, B. S.; Catalano, T.; Bozek, J. D. *J. Chem. Phys.* **2002**, *117*, 7738−7744.
(23) Amusia, M. Y.; Cherepkov, N. A.; Chernysheva, L. V.; Manson, S. T. *Phys. Rev. A* **2000**, *61*, 020701.
(24) Faubel, M.; Kisters, Th. *Nature (London)* **1989**, *339*, 527.
(25) Faubel, M.; Steiner, B.; Toennies, J. P. *J. Electron Spectrosc. Relat. Phenom.* **1998**, *95*, 159.
(26) Weber, R. Ph.D. Thesis, Freie Universität Berlin, Germany, 2003.
(27) From NIST atomic spectra database, http://www.nist.gov.
(28) Lide, D. R. *Handbook of Chemistry and Physics*; CRC Press: Boca Raton, FL, 1997−1998.
(29) Langer, B.; Viefhaus, J.; Hemmers, O.; Menzel, A.; Wehlitz, R.; Becker, U. *Phys. Rev. A* **1991**, *43*, 1652.
(30) Süzer, S.; Breuckmann, B.; Theodosiu, C. E.; Mehlhorn, W. *J. Phys. B: At. Mol. Opt. Phys.* **1980**, *13*, 2061.
(31) Meyer, M.; van Raven, E.; Sonntag, B.; Hansen, J. E. *Phys. Rev. A* **1994**, *49*, 3685.
(32) Godehusen, K. Private communication.
(33) Benson, J. M.; Nowak, I.; Potts, A. W. *J. Phys. B: At. Mol. Opt. Phys.* **1987**, *20*, 6257.
(34) Nahon, L.; Duffy, L.; Morin, P.; Combet-Fanoux, F.; Tremblay, J.; Larzilliere, M. *Phys. Rev. A* **1990**, *41*, 4879.
(35) Nahon, L.; Svensson, A.; Morin, P. *Phys. Rev. A* **1991**, *43*, 2328.
(36) Richter, M.; Bizau, J. M.; Cubaynes, D.; Menzel, T.; Wuilleumier, F. J.; Carré, B. *Europhys. Lett.* **1990**, *12*, 35.
(37) Born, M. *Z. Phys.* **1920**, *1*, 45.
(38) Marcus, Y. *Pure Appl. Chem.* **1987**, *59*, 1093.
(39) Babu, C. S.; Lim, C. *J. Chem. Phys.* **2001**, *114*, 889.
(40) Wiberg, N. *Lehrbuch der Anorganischen Chemie*, 101st ed.; de Gruyter: Berlin and New York, 1995.
(41) Jungwirth, P.; Tobias, D. J. *J. Phys. Chem. B* **2000**, *104*, 7702.
(42) Debye, P.; Hückel, E. *Z. Phys.* **1923**, *24*, 185.
(43) Adamson, A. W. *Physical Chemistry of Surfaces*, 5th ed.; J. Wiley: New York, 1990.
(44) Bradforth, S.; Jungwirth, P. *J. Phys. Chem. A* **2002**, *106*, 1286.
(45) Hertel, I. V.; Hüglin, C.; Nitsch, C.; Schulz, C. P. *Phys. Rev. Lett.* **1991**, *67*, 1767.
(46) Barnett, R. N.; Landman, *Phys. Rev. Lett.* **1993**, *70*, 1775.
(47) Misaizu, F.; Tsukamoto, K.; Sanekata, M.; Fuke, K. *Chem. Phys. Lett.* **1992**, *188*, 241.
(48) Markovich, G.; Pollack, S.; Giniger, R.; Cheshnovsky, O. *J. Chem. Phys.* **1994**, *101*, 9344.